

Object Segmentation for Linearly Polarimetric Passive Millimeter Wave Images Based on Principal Component Analysis

Xuan Lu¹, Furong Peng^{*},¹, Guanghui Li¹, Zelong Xiao², and Taiyang Hu³

Abstract—Traditional passive millimeter wave imaging (PMMW) mechanism measures intensity-only radiometric energy of the scene, and the limited information restricts the subsequent process of target detection and recognition. Polarimetric phenomena provide an extra dimension of information and are utilized to improve the PMMW imaging performance. Based on linear polarization characteristics for terrain identification in our previous work, the horizontal, vertical and 45 degree linearly polarimetric images are obtained by manually changing the polarization orientation of the radiometer with a self-designed rotating installation. Then the related Stokes parameters and the linearly polarized angle are calculated for principal component analysis (PCA). Pixels with similar polarimetric characteristic are clustered in the score-plot feature space. Then the clusters are extracted to realize object segmentation of the raw image. Three types of objects including metallic stuff, lawn and concrete park are finally segmented, demonstrating that the proposed segmentation is feasible and effective.

1. INTRODUCTION

Passive millimeter wave (PMMW) imaging technique is widely used in scene surveillance, homeland security of concealed object detection (CWD) [1, 2] and remote sensing due to its all-weather working ability, good penetrating performance, and high temperature contrast in outdoor environment [3, 4]. Polarimetric PMMW images provide an extra dimension of information beyond intensity-only radiometric energy of the scene [5, 6], thus a number of researchers are working on passive polarimetric imager design. Some of them have successfully achieved the fully-polarimetric devices [7–9], while others mainly focus on linearly (especially horizontal and vertical) polarized system due to the expensive hardware cost [10–15]. In previous work [16–18], we fixed a mechanically scanned single pixel 94GHz radiometric imaging system. The radiometer is assembled with a Cassegrain antenna fed by a linearly polarized horn, and is conically scanned in azimuth-elevation coordination to realize large view imaging. A self-designed rotating fixture shown in Fig. 1 helps to manually change the direction of the horn, and the angle scale enables quantitative rotation to achieve any linear polarization. With this device in [18], we experimentally researched linear polarization characteristics of various terrains at W-band, and obtained a group of horizontal, vertical and linearly 45 degree polarized radiometric images for a car-park. In this paper, we propose a multi-image method for subsequent image processing work. Stokes parameters related to linear polarization and the linearly polarized angle is calculated and analyzed. Principal component analysis (PCA) [19] is utilized for object segmentation of the images. In PCA eigenvector score plot, pixels with similar polarimetric characteristics of the Stokes parameters or the linear polarization angle distribute closely and form a cluster. The clusters are segmented and extracted on the score plot to realize object segmentation for the imaged view.

Received 8 August 2017, Accepted 18 October 2017, Scheduled 28 October 2017

* Corresponding author: Furong Peng (pengfr@sxu.edu.cn).

¹ Department of Electronic Information Engineering, Shanxi University, Taiyuan 030006, China. ² School of Electronic and Optical Engineering, Nanjing University of Science and Technology, Nanjing 210094, China. ³ China Academy of Space Technology (Xi'an), Xi'an 710100, China.

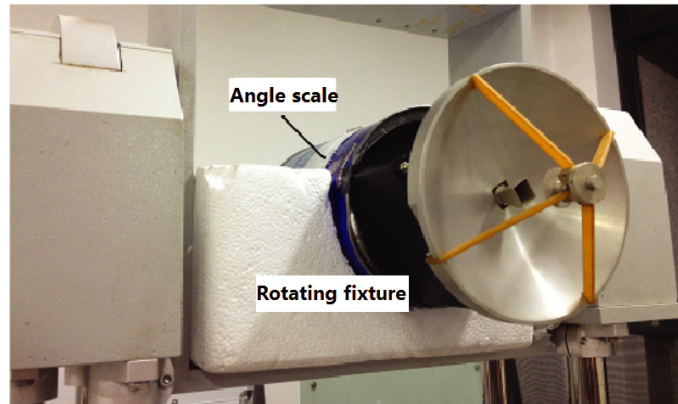


Figure 1. The 94 GHz radiometer with the self-designed rotating fixture.

2. STOKES PARAMETERS AND LINEARLY POLARIZED IMAGES

The reason we choose the park shown in Fig. 2(a) for the tested view is that it includes several most typical objects in PMMW detecting fields. The linearly polarized PMMW images shown in Figs. 2(b)~2(d) are measured in the same overlooking observation with the height about 10 m. The azimuth angle is ranged from -15° to 25° stepped by 0.1° , while the elevation angle is from 6° to

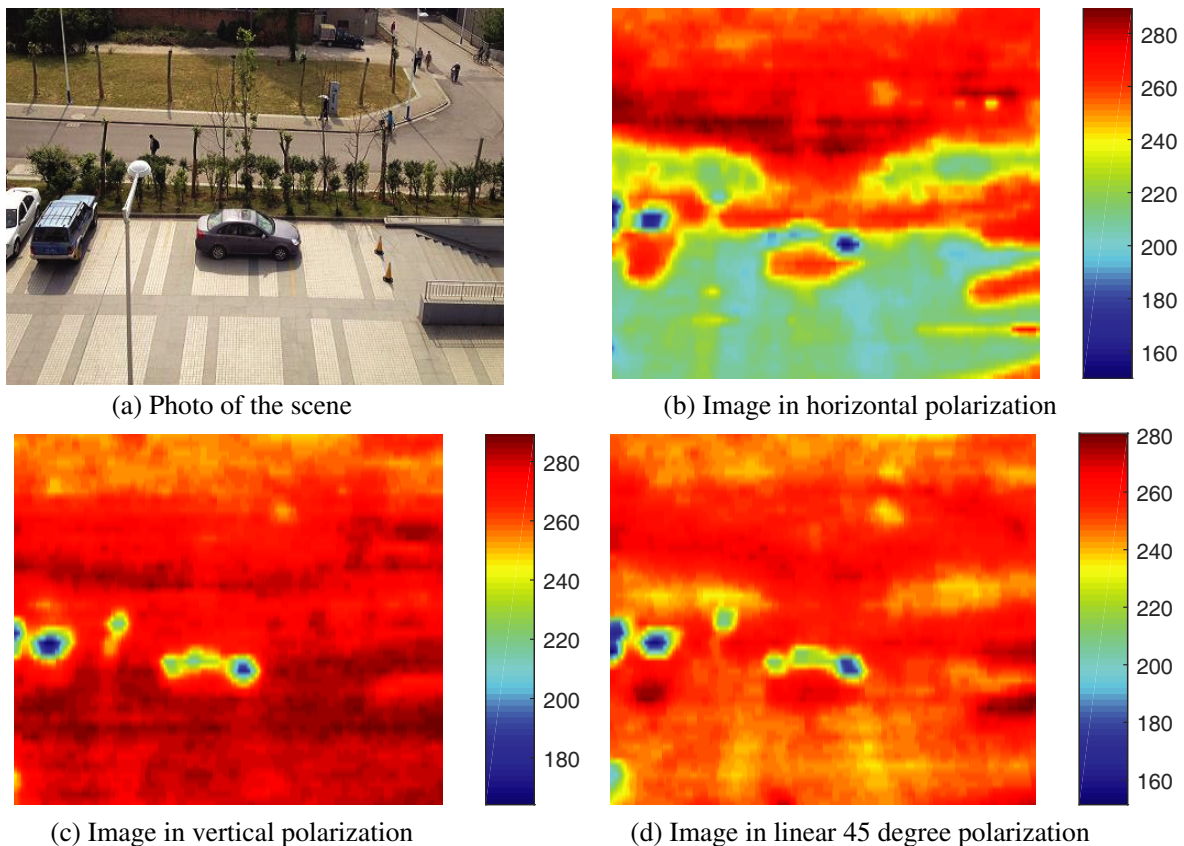


Figure 2. The optical Photo of the car-park and a group of overlooking PMMW images measured in different linear polarizations: (a) photo of the scene, (b) image in horizontal polarization, (c) image in vertical polarization, and (d) image in linear 45 degree polarization.

45° with the step of 0.5° to observe polarization difference. For the real aperture antenna, the spatial resolution is proportional to the range with the ratio of antenna beam width of 1.5°. Correspondingly, the spatial resolution of the pixels in the image is ranged from 0.26 m to 0.37 m. Comparing the four pictures, it can be seen that:

- (1) The PMMW images are of lower resolution than the optical photo and present different intensities with different polarizations;
- (2) The concrete park and asphalt road display large intensity difference between horizontal and vertical polarizations;
- (3) The street lampshade and cars are of steady low temperatures, as the metallic stuff almost completely reflects the “cold” sky temperature in all polarizations;
- (4) As for the lawn, it appears in high temperatures in every polarization because of its low reflectivity caused by diffuse reflection;
- (5) In Figs. 2(b) and 2(d), the mirror images of the short walls below iron railings and particularly the cars are obviously visible, indicating that the concrete park has smooth surface of high reflectivity at millimeter-wave band.

The PMMW image is generally represented in thermodynamic temperature. Denote the above raw data as T_H , T_V and T_{45} , where the subtitle of H , V , and 45 are respectively shorted for horizontal, vertical, and 45° linear polarizations, and we can calculate the first three Stokes parameters in Eq. 1[8].

$$\begin{aligned} S_0 &= T_H + T_V \\ S_1 &= T_H - T_V = 2T_H - S_0 \\ S_2 &= T_{45} - T_{-45} = 2T_{45} - S_0 \\ S_3 &= T_{RHC} - T_{LHC} = 2T_{RHC} - S_0 \end{aligned} \quad (1)$$

Stokes parameters can completely describe all polarizations of the radio wave, in which S_0 denotes the total radiometric intensity in all polarizations, S_1 the difference between horizontal and vertical intensities, S_2 the difference between 45° and -45° polarizations, and S_3 the difference between right-handed circulated intensity R_{RHC} and left-handed intensity R_{LHC} . The circulated polarizations are not discussed in this paper, and the linearly polarized angle

$$\alpha = \frac{1}{2} \arctan \frac{S_2}{S_1} \quad (2)$$

is also computable as S_1 and S_2 are known. Fig. 3 shows the calculated first three Stokes parameters and the linearly polarized angle of the scene.

In Fig. 3(a), the total radiometric intensity of the scene is illustrated, and it is obvious that the metallic objects of the cars and the street lampshade appear in a very low temperature, and the lawn appears in the highest temperature in contrast. The mirror images of the cars and short walls can be identified from its background of the concrete park. Fig. 3(b) shows the difference between horizontal and vertical polarizations, and the concrete park and asphalt road are featured in this view. From the Stokes parameter S_2 of Fig. 3(c), the big temperature difference mainly occurs at the edge of the non-planar object such as the cars, which is verified in Fig. 3(d). This is because the millimeter waves are diffracted instead of reflected at these locations.

3. PRINCIPAL COMPONENT ANALYSIS

At this stage, we have obtained a set of images of the park, including the linearly polarized PMMW temperatures, corresponding Stokes parameters and the linearly polarized angle. PCA is an expert in converting a set of possibly linearly-correlated observations into a set of values of linearly-uncorrelated variables called principal components (PCs). It is essentially an orthogonal linear transformation, which is usually used for dimension reduction. The property of the transformation is that the first PC has the largest possible variance, and each succeeding PC in turn has the highest variance possible under the constraint that it is orthogonal to the preceding PCs [19].

Assume the raw images and the Stokes parameter images as a data set of x_i , $i = 1, 2, \dots, N$, $x_i \in \mathbf{R}^d$, where $d = 6$ for dimensions of T_H , T_V , T_{45} , S_0 , S_1 , and S_2 , and N for the pixel number of each image.

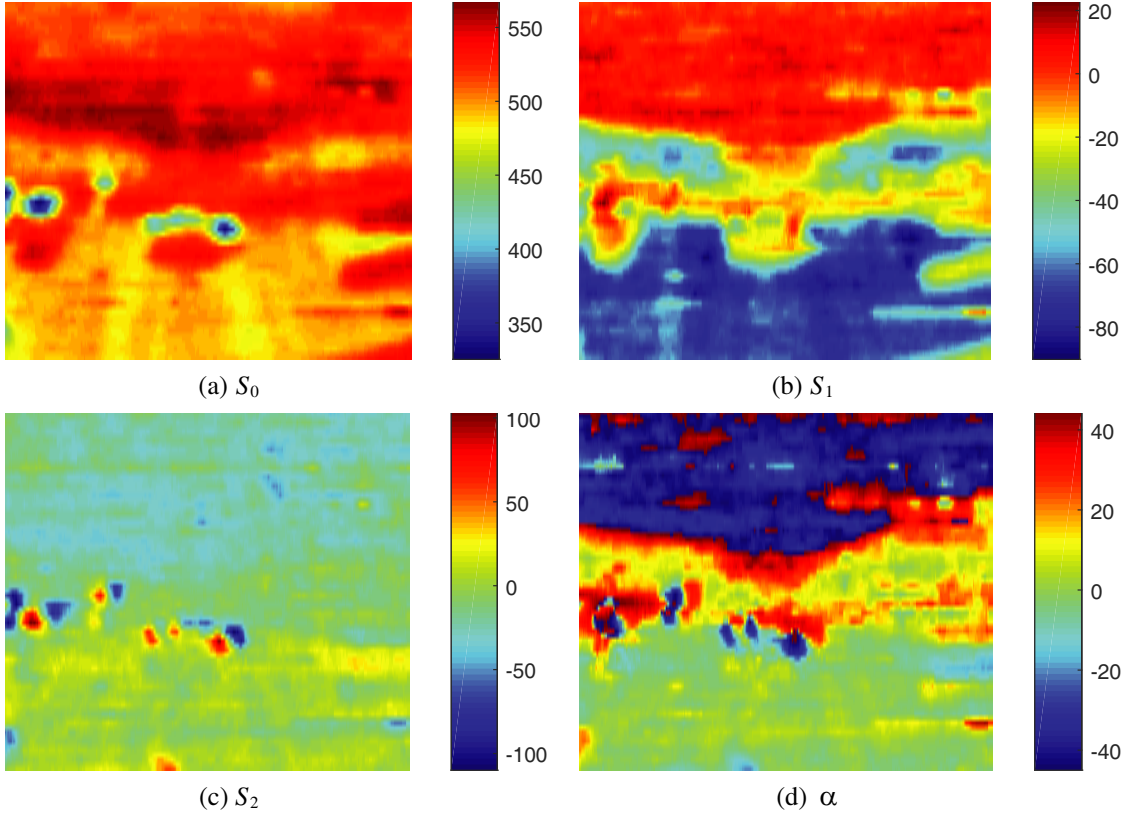


Figure 3. Stokes parameters and the linearly polarized angle of the scene: (a) S_0 , (b) S_1 , (c) S_2 , and (d) α .

According to the observation range and interval, here $N = 501 \times 79$, and all the images are resized to $N \times 1$. Mathematically, the PCA process is searching a group of optimal orthogonal unit vectors via linear transformation such that

$$C_x = U\Lambda U^T, \quad (3)$$

where

$$\begin{aligned} C_x &= E[(x - E(x))(x - E(x))^T] \\ &= \frac{1}{N} \sum_{i=1}^N (x_i - m_x)(x_i - m_x)^T \end{aligned} \quad (4)$$

$$m_x = E[x] = \frac{1}{N} \sum_{i=1}^N x_i$$

are covariance matrix and mean vector of the data set, respectively; $U = [u_1, u_2, \dots, u_d]$ represents eigenvector matrix of the covariance matrix; $\Lambda = \text{diag}([\lambda_1, \lambda_2, \dots, \lambda_d]^T)$ represents eigenvalue matrix, satisfying $\lambda_1 \geq \lambda_2 \geq \dots \geq \lambda_d$. u_i is the eigenvector corresponding to i -th maximum eigenvalue λ_i . Then PC i is the projection from matrix $X = [x_1, x_2, \dots, x_N]$ onto u_i .

$$PC_i = Xu_i, \quad (5)$$

4. IMAGE SEGMENTATION BASED ON PCA

Because Stokes parameters in Eq. 1 are essentially linear combinations of the polarized temperatures, the calculated eigenvalue matrix has only three non-zero values, corresponding to three principal components

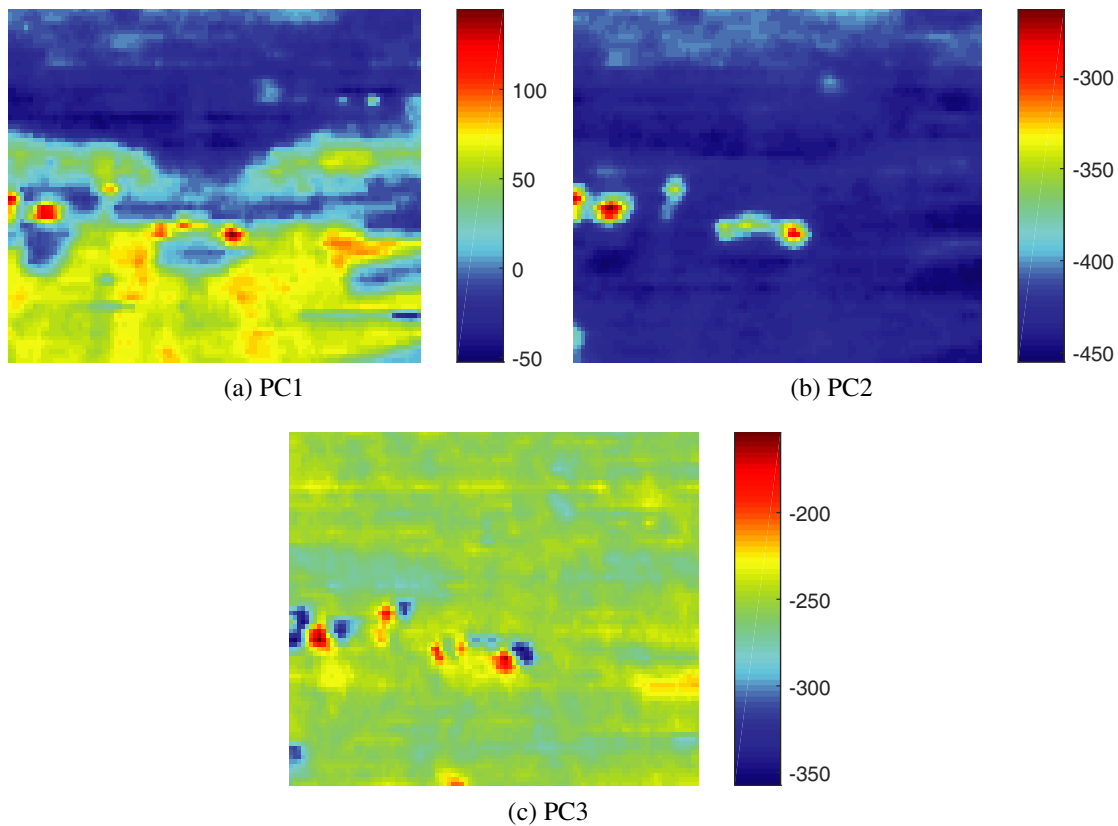


Figure 4. Principal components of the data set: (a) PC1, (b) PC2, and (c) PC3.

of PC1, PC2, PC3. As shown in Fig. 4, PC1 contains the most energy of the data set and shows an overall intensity characteristics, PC2 mainly highlights the areas of metallic objects, and PC3 features radiometric difference among various terrains. All characteristics of the raw data are remained during PCA process.

Score plot is a point-by-point statistical means that helps to reveal principal component features among multiple pixels. Its horizontal and vertical coordinates are two selected principal components respectively. Each pixel would be positioned in the score plot coordinate according to its principal component values. Pixels with similar values for both selected principal components are clustered in the score plot, i.e., they are pixels of the same feature. If these clusters are segmented, the categories of objects are separated from their background. In this paper, we add the linearly polarized angle α to the score plot coordinates, and draw the following four plots shown in Fig. 5.

The features of the images are involved in score plot by density of the point. Generally speaking, the dense area is corresponding to the background pixels, while the sparse areas are more likely image details. For example in Fig. 5(a) of PC3-PC1, all the points are basically clustered in two sides of the dotted lines, corresponding to the backgrounds of lawn and the concrete park respectively in the real scene. This is because the intensity of PC1 is almost the same, while two backgrounds are easily distinguished in PC3. We totally extract three clusters of points, which we label as C1, C2 and C3 in Figs. 5(b)~5(d). Relocating these pixels to image space in Fig. 6, it is obvious that C1 and C3 clusters represent the lawn and the concrete terrains respectively, and C2 cluster is for the metallic objects of cars and the street lampshade. This result is consistent with what can be clearly seen in Fig. 2, indicating the correctness and effectiveness of the segmentation. The reason why we use PCA instead of straightly processing Fig. 2 is mainly for the following considerations:

- (1) For scene-based image processing method like threshold segmentation and edge detection, the features are based on the relationship between different pixels in one image. While working on multi-image process problem, it is defective as it ignores the features reflected at a certain pixel in

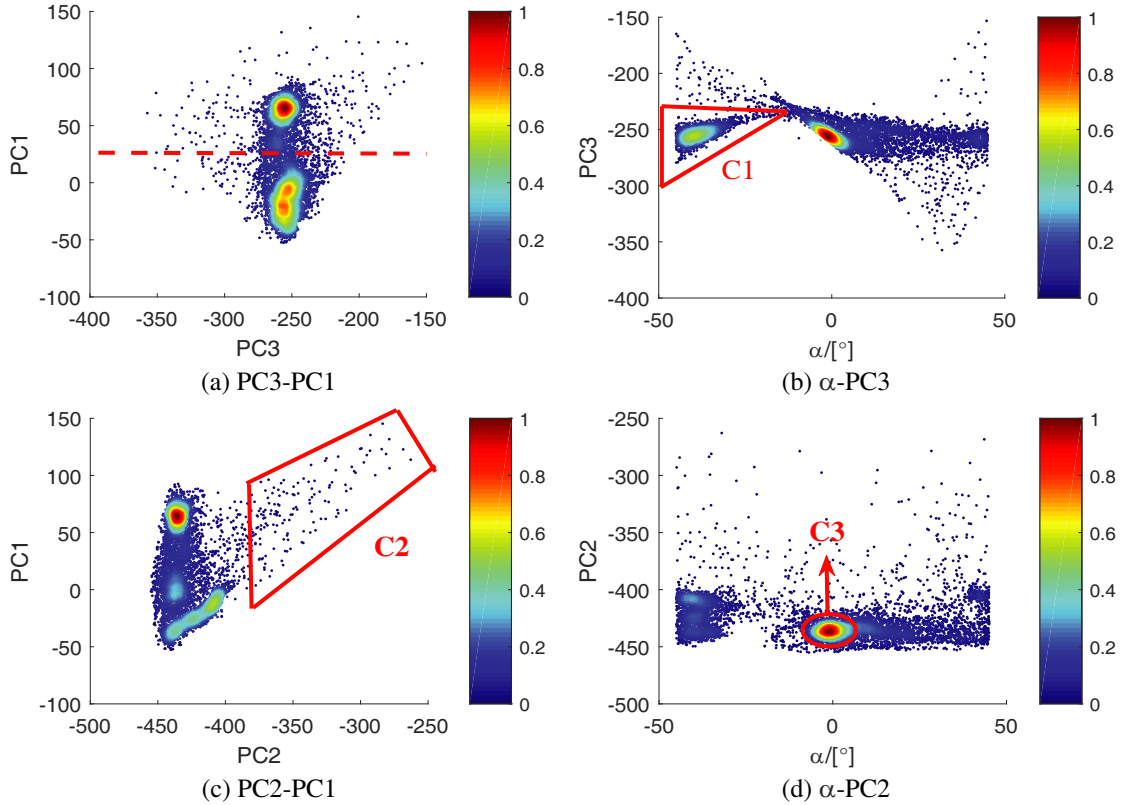


Figure 5. PCA score plots: (a) PC3-PC1, (b) α -PC3, (c) PC2-PC1, and (d) α -PC2.

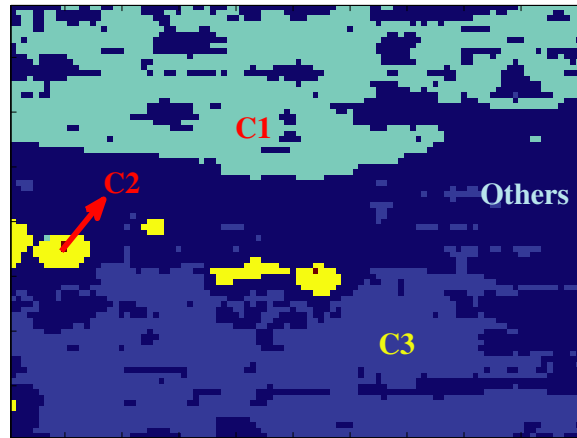


Figure 6. Segmentation result.

different images. As a result, a false metallic object of puddle, which displays similar radiometric temperature in horizontal polarization but a higher temperature in vertical polarization, would be wrongly segmented for example.

(2) Both threshold segmentation and edge detection methods involve a lot of parameter selection stuff, which may cause different results. Besides, edge detection is generally sensitive to noise, and the obtained edge is usually discontinuous.

(3) In many situations, it is required to deal with large number of images, and PCA method is expert in dimension reduction.

5. CONCLUSION

This paper proposes an effective object segmentation approach for linearly polarimetric PMMW images based on PCA method. Objects present different polarization characteristics due to their own inherent attributes, and these characteristics can be extracted and utilized to improve detection and recognition performance of PMMW imaging system. Restricted by our available hardware condition, the circulated polarization is not involved to realize full-polarized imaging in this paper. We believe that the full-polarization technique is future development trend, and it is also what our next research will focus on.

ACKNOWLEDGMENT

This work is supported by the National Natural Science Foundation of China (No. 61501234), and 2016 Shanxi Provincial Startup Foundation for Advanced Talents (No. 127546003).

REFERENCES

1. Isiker, H., C. Ozdemir, and I. Unal, "Millimeter-wave band radiometric imaging experiments for the detection of concealed objects," *2015 IEEE Radar Conference*, 23–26, Johannesburg, 2015.
2. Chen, H.-M., S. Lee, R. M. Rao, M. A. Slamani, and P. K. Varshney, "Imaging for concealed weapon detection: A tutorial overview of development in imaging sensors and processing," *IEEE Signal Processing Magazine*, Vol. 22, No. 2, 52–61, 2005.
3. Yujiri, L., "Passive millimeter wave imaging," *2006 IEEE MTT-S International Microwave Symposium Digest*, 98–101, 2006.
4. Manabu, I., N. Shunichi, and N. Tatsuo, "Near-field thermal imaging by passive millimeter-wave microscopy," *2014 Asia-Pacific Microwave Conference, APMC*, 1034–1036, 2014.
5. Zrazhevskij, A. Y., V. A. Golunov, D. M. Ermakov, M. T. Smirnov, E. P. Novichikhin, S. P. Golovachev, and E. V. Konkov, "The development of radiophysical methods for the polarization, including stereo) images acquisition in millimeter range related to problems of objects recognition, navigation, emergency management, security control and antiterroristic activity," *Proceedings of IEEE International Geoscience and Remote Sensing Symposium*, 2258–2261, 2005.
6. Nghiem, S. V., M. E. Veysoglu, J. A. Kong, and R. T. Shin, "Polarimetric passive remote sensing of a periodic soil surface: Microwave measurements and analysis," *Journal of Electromagnetic Waves and Applications*, Vol. 5, No. 9, 997–1005, 1991.
7. Bernacki, B. E., J. F. Kelly, D. M. Sheen, D. L. McMakin, J. R. Tedeschi, T. E. Hall, B. K. Hatchell, and P. L. J. Valdez, "Phenomenology studies using a scanning fully polarimetric passive W-band millimeter wave imager," *SPIE Proceedings: Passive and Active Millimeter-Wave Imaging XIV*, 80220C1–80220C10, 2011.
8. Wikner, D. A. and G. Samples, "Polarimetric passive millimeter-wave sensing," *SPIE Proceedings: Passive Millimeter-Wave Imaging Technology V*, 86–93, 2011.
9. Bernacki, B. E., J. F. Kelly, D. M. Sheen, D. L. McMakin, J. R. Tedeschi, R. V. Harris, A. Mendoza, T. E. Hall, B. K. Hatchell, and P. L. J. Valdez, "Passive fully polarimetric W-band millimeter-wave imaging (Invited Paper)," *SPIE Proceedings: RF and Millimeter-Wave Photonics II*, 82590F1–82590F11, 2012.
10. Liao, S., N. Gopalsami, T. W. Elmer, E. R. Koehl, A. Heifetz, K. Avers, E. Dieckman, and A. C. Raptis, "Passive millimeter-wave dual-polarization imagers," *IEEE Transactions on Instrumentation and Measurement*, Vol. 61, No. 7, 2042–2050, 2012.
11. Wilson, J. P., C. A. Schuetz, E. L. Stein, Jr., J. P. Samluk, D. G. Mackrides, and D. W. Prather, "Polarization difference imaging for millimeter-wave in a desert environment," *SPIE Proceedings: Millimeter-Wave and Terahertz Sensors and Technology III*, 78370E1–78370E6, 2012.

12. Gopalsami, N., S. Liao, T. Elmer, E. R. Koehl, and A. C. Raptis, "Evaluation of passive millimeter wave system performance in adverse weather conditions," *SPIE Proceedings: Passive and Active Millimeter-Wave Imaging XV*, 83620I1-83620I6, 2012.
13. Yeom, S., D.-S. Lee, H. Lee, J.-Y. Son, and V. P. Guschin, "Vector clustering of passive millimeter wave images with linear polarization for concealed object detection," *Progress In Electromagnetics Research Letters*, Vol. 39, 169–180, 2013.
14. Wilson, J. P., C. A. Schuetz, C. E. Harrity, S. Kozacik, D. L. K. Eng, and D. W. Prather, "Measured comparison of contrast and crossover periods for passive millimeter-wave polarimetric imagery," *Optics Express*, Vol. 21, No. 10, 12899–12906, 2013.
15. Kim, W.-G., N.-W. Moon, H.-K. Kim, and Y.-H. Kim, "Linear polarization sum imaging in passive millimeter-wave imaging system for target recognition," *Progress in Electromagnetics Research*, Vol. 136, 175–193, 2013.
16. Lu, X., Z. Xiao, J. Xu, and H. Huo, "3D millimeter wave image by combined active and passive system," *Progress In Electromagnetics Research Letters*, Vol. 50, 7–12, 2014.
17. Lu, X., L. Wu, Z. Xiao, and J. Xu, "Ranging technique based on conically scanned single pixel millimeter wave radiometer," *International Journal of Engineering Research in Africa*, Vol. 12, 43–52, 2014.
18. Lu, X., Z. Xiao, and J. Xu, "Linear polarization characteristics for terrain identification at millimeter wave band," *Chinese Optics Letters*, Vol. 12, No. 10, 1012011–1012015, 2014.
19. Prats-Montalbana, J. M., A. de Juanb, and A. Ferrera, "Multivariate image analysis: A review with applications," *Chemometrics and Intelligent Laboratory Systems*, Vol. 107, No. 1, 1–23, 2011.